ORCA – Online Research @ Cardiff

Validating the RedMIT/GFP-LC3 mouse model by studying mitophagy in Autosomal Dominant Optic Atrophy due to the OPA1Q285STOP mutation.

Alan Diot[1, 2], Thomas Agnew[3], Jeremy Sanderson[3], Chunyan Liao[4], Janet Carver[1, 2], Ricardo Neves[5], Rajeev Gupta[6], Yanping Guo[7], Caroline Waters[8], Sharon Seto[8], Matthew Daniels[9], Eszter Dombi[1, 2], Tiffany Lodge[1, 2], Karl Morten[1, 2], Suzannah Williams[2], Tariq Enver[6], Francisco J. Iborra[10], Marcela Votruba[8], Joanna Poulton[1, 2*]

[1]Nuffield Department of Obstetrics and Gynaecology, University of Oxford, United Kingdom, [2]Nuffield department of women's and reproductive health, University of Oxford, United Kingdom, [3]Mammalian Genetics Unit and Mary Lyon Centre, Medical Research Council Harwell (MRC), United Kingdom, [4]Molecular Biology & Biotechnology, University of Sheffield, United Kingdom, [5]Centro de Neurociências e Biologia Celular, Universidade de Coimbra, Portugal, [6]University College London, United Kingdom, [7]National Heart and Lung Institute, Imperial College London, United Kingdom, [8]School of Optometry and Vision Sciences, Cardiff University, United Kingdom, [9]Division of Cardiovascular Medicine, Radcliffe Department of Medicine, Nuffield Department of Medicine, Medical Sciences Division, University of Oxford, United Kingdom, [10]CSIC, Centro Nacional de Biotecnología (CNB), Spain

Conflict of interest statement

The authors declare that the research was conducted in the absence of any commercial or financial relationships that could be construed as a potential conflict of interest

Author contribution statement

AD, TA, JS, CL, JC, RN, RG, YG, CW, SS, MD, ED, LM performed the experiments. JP, KM and AD designed the experiments. JP, JS, RC, TL, FI, KM and AD analyzed the results. JP, AD, JS, KM and MD wrote this manuscript.

Keywords

mitophagy, mouse model, OPA1, adOA, Mitochondrial fragmentation, high content imaging

Abstract

Word count: 350

Background
Autosomal dominant optic atrophy (ADOA) is usually caused by mutations in the essential gene, OPA1. This encodes a ubiquitous protein involved in mitochondrial dynamics, hence tissue specificity is not understood. Dysregulated mitophagy (mitochondria recycling) is implicated in ADOA, being increased in OPA1 patient fibroblasts. Furthermore, autophagy may be increased in retinal ganglion cells of the OPA1Q285STOP mouse model.

Aims
We developed a mouse model for studying mitochondrial dynamics in order to investigate mitophagy in ADOA.

Methods
We crossed the OPA1Q285STOP mouse with our RedMIT/GFP-LC3 mouse, harboring red fluorescent mitochondria and green fluorescent autophagosomes. Colocalization between mitochondria and autophagosomes, the hallmark of mitophagy, was quantified in fluorescently labelled organelles in primary cell cultures, using two high throughput imaging methods (Imagestream (Amnis) and IN Cell Analyzer 1000 (GE Healthcare Life Sciences)). We studied colocalisation between mitochondria and autophagosomes in fixed sections using confocal microscopy.

Results
We validated our imaging methods for RedMIT/GFP-LC3 mouse cells, showing that colocalization of red fluorescent mitochondria and green fluorescent autophagosomes is a useful indicator of mitophagy. We showed that colocalization increases when lysosomal processing is impaired. Further, colocalization of mitochondrial fragments and autophagosomes is increased in cultures from the OPA1Q285STOP/RedMIT/GFP-LC3 mice compared to for RedMIT/GFP-LC3 control mouse cells that were wild type for OPA1. This was apparent in both mouse embryonic fibroblasts using IN Cell 1000 and in splenocytes using ImageStream imaging flow cytometer (Amnis). We confirmed that this represents increased mitophagic flux using lysosomal inhibitors. We also used microscopy to investigate the level of mitophagy in the retina from the OPA1Q285STOP/RedMIT/GFP-LC3 mice and the RedMIT/GFP-LC3 control mice. However, the expression levels of endogenous fluorescent proteins and the image signal-to-noise ratios precluded the detection of colocalisation so we were unable to show any difference in colocalization between these mice.

Conclusions
We show that colocalization of fluorescent mitochondria and autophagosomes in cell cultures, but not fixed tissues from the RedMIT/GFP-LC3, can be used to detect mitophagy. We used this model to confirm that mitophagy is increased in a mouse model of ADOA. It will be useful for cell based studies of diseases caused by impaired mitochondrial dynamics.

Funding statement

Ethics statements

(Authors are required to state the ethical considerations of their study in the manuscript, including for cases where the study was exempt from ethical approval procedures)

Does the study presented in the manuscript involve human or animal subjects: Yes

Please provide the complete ethics statement for your manuscript. Note that the statement will be directly added to the manuscript file for peer-review, and should include the following information:

- Full name of the ethics committee that approved the study
- Consent procedure used for human participants or for animal owners
- Any additional considerations of the study in cases where vulnerable populations were involved, for example minors, persons with disabilities or endangered animal species

As per the Frontiers authors guidelines, you are required to use the following format for statements involving human subjects:
This study was carried out in accordance with the recommendations of [name of guidelines], [name of committee]. The protocol was approved by the [name of committee]. All subjects gave written informed consent in accordance with the Declaration of Helsinki.
For statements involving animal subjects, please use:
This study was carried out in accordance with the recommendations of 'name of guidelines, name of committee'. The protocol was approved by the 'name of committee'.

If the study was exempt from one or more of the above requirements, please provide a statement with the reason for the exemption(s).
Ensure that your statement is phrased in a complete way, with clear and concise sentences.

This study was carried out in accordance with the United Kingdom's Home Office protocols, covered by the Animals (Scientific Procedures) Act 1986.
The protocol was approved by the Oxford University Committee on Animal Care and Ethical Review, University of Oxford Medical Sciences division (Project licences 3002208 and 3003213).

Validating the RedMIT/GFP-LC3 mouse model by studying mitophagy in Autosomal Dominant Optic Atrophy due to the OPA1Q285STOP mutation.

Alan Diot[1], Thomas Agnew[2], Jeremy Sanderson[2], Chunyan Liao[3], Janet Carver[1], Ricardo Neves[4], Rajeev Gupta[5], Yanping Guo[6], Caroline Waters[7], Sharon Seto[7], Matthew J Daniels[8], Eszter Dombi[1], Tiffany Lodge[1], Karl Morten[1], Susannah Williams[1], Tariq Enver[5], Francisco Iborra[9], Marcela Votruba[7] and Joanna Poulton[1*]

[1]Nuffield Department of Obstetrics and Gynaecology, University of Oxford
[2] MRC Harwell Institute, Mammalian Genetics Unit and Mary Lyon Centre, Harwell Campus, Oxfordshire
[3] Molecular Biology & Biotechnology, University of Sheffield
[4] Centro de Neurociências e Biologia Celular (CNC), Coimbra, Portugal
[5] University College London, London
[6] National Heart and Lung Institute, Imperial College London, London, United Kingdom
[7] School of Optometry and Vision Sciences, Cardiff University
[8] Division of Cardiovascular Medicine, Radcliffe Department of Medicine, University of Oxford.
[9] Centro Nacional de Biotecnología, CSIC, Madrid, Spain

* Correspondence:
Joanna Poulton
joanna.poulton@obs-gyn.ox.ac.uk

Abstract

Background

Autosomal dominant optic atrophy (ADOA) is usually caused by mutations in the essential gene, OPA1. This encodes a ubiquitous protein involved in mitochondrial dynamics, hence tissue specificity is not understood. Dysregulated mitophagy (mitochondria recycling) is implicated in ADOA, being increased in OPA1 patient fibroblasts. Furthermore, autophagy may be increased in retinal ganglion cells of the OPA1^{Q285STOP} mouse model.

Aims

We developed a mouse model for studying mitochondrial dynamics in order to investigate mitophagy in ADOA.

Methods

We crossed the OPA1^{Q285STOP} mouse with our RedMIT/GFP-LC3 mouse, harboring red fluorescent mitochondria and green fluorescent autophagosomes. Colocalisation between mitochondria and autophagosomes, the hallmark of mitophagy, was quantified in fluorescently labelled organelles in primary cell cultures, using two high throughput imaging methods Imagestream (Amnis) and IN Cell Analyzer 1000 (GE Healthcare Life Sciences). We studied colocalisation between mitochondria and autophagosomes in fixed sections using confocal microscopy.

47
48 **Results**
49 We validated our imaging methods for RedMIT/GFP-LC3 mouse cells, showing that colocalisation
50 of red fluorescent mitochondria and green fluorescent autophagosomes is a useful indicator of
51 mitophagy. We showed that colocalisation increases when lysosomal processing is impaired.
52 Further, colocalisation of mitochondrial fragments and autophagosomes is increased in cultures from
53 the OPA1^{Q285STOP}/RedMIT/GFP-LC3 mice compared to RedMIT/GFP-LC3 control mouse cells that
54 were wild type for OPA1. This was apparent in both mouse embryonic fibroblasts using IN Cell
55 1000 and in splenocytes using ImageStream imaging flow cytometer (Amnis). We confirmed that
56 this represents increased mitophagic flux using lysosomal inhibitors. We also used microscopy to
57 investigate the level of mitophagy in the retina from the OPA1^{Q285STOP}/RedMIT/GFP-LC3 mice and
58 the RedMIT/GFP-LC3 control mice. However, the expression levels of fluorescent proteins and the
59 image signal-to-background ratios precluded the detection of colocalisation so we were unable to
60 show any difference in colocalisation between these mice.
61
62 **Conclusions**
63 We show that colocalisation of fluorescent mitochondria and autophagosomes in cell cultures, but not
64 fixed tissues from the RedMIT/GFP-LC3, can be used to detect mitophagy. We used this model to
65 confirm that mitophagy is increased in a mouse model of ADOA. It will be useful for cell based
66 studies of diseases caused by impaired mitochondrial dynamics.

Introduction

Mitochondria are important for cells, not just for generating energy, calcium regulation and key biosynthetic processes including synthesis of iron Sulphur centres, but also for apoptosis, signaling and response to cellular stress (Suomalainen and Battersby, 2018). Mitochondria form a dynamic reticulum in cells, with portions of this network constantly fusing and dividing (Legros et al., 2002). Mitochondrial location and transport are particularly important in neurons, individual mitochondria moving along microtubules in the cytoplasm to synapses and other parts of the cell requiring energy (Li et al., 2004). These dynamics are under the control of molecular players such as Drp1 and Fis1 for fission and mitofusins (Legros et al., 2002) and OPA1 for fusion (Chen and Chan, 2006). Hence mitochondrial diseases are mechanistically diverse and do not necessarily manifest clear evidence of impaired ATP synthesis. For instance, the evidence for respiratory chain dysfunction in mitochondrial optic neuropathies may be very subtle (Yu-Wai-Man et al., 2002). Nevertheless, these are important diseases that impair vision, resulting in lifelong disability.

Exactly how mutations in both mitochondrial DNA (mtDNA), encoding subunits of the respiratory chain and in nuclear genes involved in mitochondrial biogenesis can cause optic neuropathies with rather similar phenotypes is poorly understood. Retinal ganglion cells (RGCs), forming the optic nerve and transmitting visual information to the brain, are the cell type that is affected in both Leber Hereditary Optic Neuropathy (LHON) and Autosomal dominant optic atrophy (ADOA) respectively. Autophagy (a type of cellular quality control) is important for the maintenance of RGCs: even a slight reduction in retinal autophagy levels can alter the capability of retinal ganglion cells to respond to axonal stress (Boya, 2017) which can be rescued by activating autophagy with rapamycin (Rodríguez-Muela et al., 2012).

ADOA is the commonest inherited optic neuropathy (prevalence 1:25 000) resulting in a bilateral, symmetrical and painless loss of vision, color vision defects, central visual field loss and atrophy of the optic disc. It is a slowly progressive neuropathy, currently irreversible and untreatable. Over 200 mutations in the essential gene OPA1 have been identified, comprising about 60% of patients with ADOA (Yu-Wai-Man et al., 2014). The OPA1 gene encodes a ubiquitous protein involved in mitochondrial dynamics. It plays a crucial role in the regulation of the mitochondrial network and cristae morphology, in oxidative phosphorylation, maintenance of mitochondrial membrane potential (MMP), in apoptosis and in neuronal maturation (Bertholet et al., 2013). Furthermore, upregulation of OPA1 can protect against some types of mitochondrial disease (Civiletto et al., 2015). We showed that mitophagy (a subtype of autophagy for maintaining mitochondrial quality) can be upregulated by OPA1 knock down (Liao et al., 2017). When knock down is profound, mitochondrial DNA (mtDNA) depletion and respiratory chain dysfunction are seen in primary cultures of fibroblasts (Liao et al., 2017) and cortical primary neurons (Bertholet et al., 2013). When OPA1 is over-expressed it can ameliorate defects in the respiratory chain (Civiletto et al., 2015; Varanita et al., 2015). We showed that mitophagy is dysregulated in fibroblasts from patients with either mitochondrial (Dombi et al., 2016) or autosomal inherited (Liao et al., 2017) optic neuropathies. We therefore sought to develop a mouse model to investigate the role of OPA1 in the mitochondrial dynamics of RGCs. We used the B6;C3-Opa1(Q285STOP) mouse which has a heterozygous mutation located in exon 8 immediately before the central dynamin-GTPase domain (Davies et al., 2007). This mutation halves the expression of OPA1 protein in all tissues, including the retina, on Western blot analysis (Davies et al., 2007). Heterozygous mutants show a slow onset of degeneration in the optic nerve, preceded by retinal ganglion cell dendropathy (Williams et al., 2010). Furthermore, the mice demonstrate a reduction in visual function on testing with the optokinetic drum and the circadian running wheel (Davies et al., 2007).

116 Dysfunctional mitochondria can be recycled by a specific type of autophagy, called mitophagy. The
117 damaged mitochondrial fragment is targeted to a developing autophagosome, called a phagophore,
118 which engulfs the mitochondrion forming a so-called "mitophagosome" (Eid et al., 2016a). This
119 then fuses with a lysosome generating a "mitophagolysosome" (Eid et al., 2016a) that acidifies and
120 degrades its contents, including the mitochondrion. Key stages in this process have been exploited to
121 highlight markers as a readout for mitophagy. For instance, both Finkel (Sun et al., 2015) and
122 Ganley (McWilliams et al., 2016) used genetically encoded fluorescent proteins, targeted to
123 mitochondria, that respond to the drop in pH following fusion with the lysosome (with mKeima and
124 mCherry respectively). These are endpoint and steady state assays, respectively. Because they both
125 depend on lysosomal acidification they are particularly useful for highlighting defects in lysosomal
126 processing, late in the mitophagy process.
127
128 We however started our studies before either of these pH sensitive models was available. In studying
129 the effects of OPA1 knock down on mitophagy we postulated that mitochondrial fragmentation
130 might drive mitophagy and hence were specifically interested in engulfat of mitochondria by
131 autophagosomes in the earliest stages of this process. We therefore exploited a tool developed by
132 Mizushima, who visualized autophagosomes by tagging their molecular hallmark, LC3-ll with green
133 fluorescent protein (GFP) (Mizushima et al., 2004). We made mice in which monomeric red
134 fluorescent protein (mRFP) was targeted to mitochondria and crossed these with Mizushima's LC3-
135 GFP mice (Mizushima et al., 2004) to visualize colocalisation of mitochondria and autophagosomes.
136 Hence we focussed on an earlier stage of mitophagy than the other two assays (Sun et al., 2015)
137 (McWilliams et al., 2016). We developed this as a readout for mitophagy driven by OPA1 knock
138 down, in which we anticipated that excessive mitochondrial fragmentation, apparent in retinal
139 ganglion cells of this mouse model (Williams et al., 2012), drives mitophagy (Liao et al., 2017).
140

Materials and methods
Media and Chemicals
143 DMEM glucose free (11966-025), DAPI (D1306) and goat anti-rabbit AlexaFluor 488 (A-11008)
144 fluorescent secondary antibodies were purchased from Life Technologies. Primary mouse anti-PDH
145 (sc-377092) antibody was purchased from SantaCruz Biotechnology. DMEM high (4.5g/L) glucose
146 (D6546), Galactose (G5388) and the pharmacological agents E64d (E8640), Pepstatin A (77170) and
147 Chloroquine (C6628) were purchased from Sigma Aldrich. Penicillin and Streptomycin (P4458) were
148 purchased from Sigma Aldrich.
149

Genetic modification of mouse embryos
151 RedMIT mice, developed by collaborator FI, express mRFP downstream of the COX VIII targeting
152 peptide, driven by the EF1α promoter (ubiquitous expression). Hence mitochondria appear red when
153 viewed by fluorescence microscopy (figure 1). Mouse ES cells (129 background) were transduced
154 with a VSV pseudotyped pHR'SIN-cPPT-SE lentivirus (Demaison et al., 2002) in which the human
155 EF1a promoter drives expression of a fusion gene containing the mitochondrial localization signal of
156 COX VIII and RFP. A clone with low RFP expression in which viability/function was not impaired
157 by RFP was selected by FACS to produce the mouse by microinjecting ES cells into embryos for
158 founders
159

Mouse Embryonic Fibroblasts production
161 A pregnant RedMIT-GFP-LC3 or RedMIT-GFP-LC3-OPA1^{Q285STOP} mouse was sacrificed on
162 embryonic day 13.5 or 14.5 and the uterine horns dissected. The excess fat was trimmed away before
163 opening the uterus carefully to release the conceptuses. The embryonic membranes and placenta were

164 removed from each embryo. The head and internal organs were removed and the remainder minced
165 as finely as possible using a sterile scalpel. It was incubated in trypsin for 5min at 37°C.
166 After a vigorous shake to dissociate the tissue, large debris were allowed to settle before the
167 supernatant was transferred to a tube containing DMEM medium + 10% FCS +
168 penicillin/streptomycin (250µM). The trypsin extraction was repeated three times and the cells split
169 into four 75cm^2 flasks. The medium was changed the following day to remove further debris. When
170 the flasks were confluent, each flask was passaged into a 175 cm^2 flask. Once confluent, these cells
171 were harvested and frozen in 1 ml aliquots at about 10^7 cells/ml for storage.
172
High-throughput microscopy and mitophagy assessment
174 For IN Cell 1000 analysis, mouse embryonic fibroblasts (MEFs) were seeded at 10^4 cells per well in
175 a Nunc F 96-well plate (Thermo Scientific) and treated in the indicated conditions for 24 hours. Cells
176 were fixed with 4% (w/v) paraformaldehyde (PFA) for 15 minutes before DAPI staining (dilution
177 1/5000 for 5 minutes). The cells were imaged using the IN Cell 1000 analyzer (500 cells acquired per
178 well) and raw images processed and parameters obtained using a previously published (Diot et al.,
179 2015) customized protocol in the IN Cell Developer toolbox (GE Healthcare Life Sciences).
180
181 We used Imagestream, which we previously validated for detecting mitophagy (Liao et al., 2017), for
182 analysis of splenocytes. Spleens were removed immediately after death and placed in individual
183 sterile dishes with 1mL of cell culture media. The spleen cells were separated out by mechanical
184 disruption and divided equally between two 25cm^3 flasks in 5mL of DMEM. Chloroquine was added
185 to a concentration of 20µM to one of the flasks and both flasks incubated overnight at 37°C. Floating
186 and trypsinized cells were filtered through a 30µm filter and fixed in 4% PFA for 15 min at room
187 temperature. After permeabilization in 0.4% Triton for 3min, cells were washed in PBS and
188 resuspended in 50-100uL of FACS buffer for analysis with Imagestream (1000-5000 cells in each
189 condition from three mice in each condition).
190 To identify colocalisation of autophagosomes and mitochondria as an indicator of mitophagy
191 we used Amnis IDEAS software, counting the numbers of LC3 positive puncta that colocalised with
192 mitochondria, using a "threshold" mask for detecting mitochondrial
193 location. Duplicate analyses using threshold masks of either 30% or 70% of the range of
194 intensity values as defined by the starting mask was used to exclude pixels.
195
Oxygen consumption measurement
197 MEFs were plated at a density of 50,000 per cells per well in black 96 well plates with clear bottoms
198 (Falcon Corning). Cells were left for 7 hours to attach and then media switched to media with
199 glucose (25mM) or galactose (10mM) and incubated in a standard 37°C - 5% CO2 incubator. A
200 parallel plate was set up for Hoechst quantification to allow normalization for cell number. After 16
201 hours media were replaced with fresh media containing the MitoXpress xtra oxygen probe (Luxcel
202 Biosciences) and overlayed with mineral oil. The oxygen consumption assay was carried on in a
203 BMG OMEGA plate reader equilibrated at 37°C and monitored for at least 4 hours. Initial oxygen
204 consumption rates (fluorescence life time) were calculated in the linear phase of the assay and
205 standardized to cell number measured using Hoechst on the parallel plate.
206
Mouse husbandry and Ethics Statement
208 All animals were housed and managed in accordance with the United Kingdom's Home Office
209 protocols, covered by the Animals (Scientific Procedures) Act 1986. The protocol was approved by
210 the Oxford University Committee on Animal Care and Ethical Review, University of Oxford Medical
211 Sciences division (Project licences 3002208 and 3003213).

212
213 Mice were housed in conventional wire-top polycarbonate cages, with a 12:12 light:dark cycle at
214 temperatures between 19-23°C and relative humidity 55±10%. Food and water were offered ad
215 libitum. The facility is free of *MHV, EDIM, MVM, MPV, PVM, Sendai, TMEV, ectomelia, LCMV,*
216 *Mad 1 and 2, MCMV, reovirus 3, Citrobacter rodentium, Clostridium piliforme, Corynebacterium*
217 *kutscheri, Mycoplasma, Pasteurellaceae, Salmonella, beta-hemolytic streptococci, Streptococcus*
218 *pneumoniae, Streptobacillus moniliformis, endoparasites* and *ectoparasites. Helicobacter* and *MNV*
219 are present in this facility.
220
221 **Confocal microscopy**
222 MEFs were plated onto 0 thickness coverslips and treated as described in the main text. 4%
223 paraformaldehyde was used for fixation (10min, room temperature). Cells were permeabilized and
224 washed in 0.1% Triton-Tris buffered saline three times before mounting on slides using Vectashield
225 (Vector Labs). Images were acquired on an upright Leica SP5 confocal microscope equipped with the
226 appropriate filters and sequential 488nm, and 568nm laser illumination.
227 For mouse eyes, four samples (2x RedMIT-GFP-LC3 and 2x RedMIT-GFP-LC3-OPA1^{Q285STOP})
228 were harvested from perfused-fixed mice and cryostat eye sections cut at 10 µm, lightly counter-
229 stained with DAPI (1:30,000 dilution; 5 minutes) and sealed using aqueous glycerol-based mountant
230 with a No. 1.5 coverslip. They were examined using a Zeiss LSM 700 inverted confocal microscope
231 with a plan-Apo 63x NA 1.4 oil-immersion objective. The optical section thickness was set at 1.0
232 micrometer, and as far as was practicable the optic nerve head was examined. The maximum Pearson
233 product moment correlation coefficient values were recorded across all four slides, using the
234 colocalisation software in the Zeiss Zen Black, Zen 2.3 SP1 version 14.0.0.0.0 with the scatter-plot
235 threshold set to three times the standard deviation of the mean value of the background pixels, as
236 investigated by Barlow et al (Barlow et al., 2010).
237
238 **Live cell imaging**
239 MEFs, cultured and treated as described above, were plated into a 35mm MatTek dish, and
240 supplemented with 10mM Hepes to buffer pH during live cell imaging. A custom Olympus IX81
241 inverted microscope equipped with temperature control (Solent scientific), LED illumination (Cairn
242 Research), a Semrock quad-band filter set (bandpass filter (DS/FF01-387/485/559/649-25), dichroic
243 quad-edge beam splitter (DS/FF410/504/582/669-Di01-25x36), and quad bandpass emission filter
244 (DS/FF01-440/521/607/700-25) and simultaneous dual image acquisition with two C-1900
245 EMCCD's (C1900, Hamamatsu, Japan) mounted after a beam splitter (Dual View C2, Photometrics)
246 controlled thorough CellR (Olympus, Japan) with a x60 oil immersion lens (Olympus, NA 1.42).
247 Simultaneous red and green images were acquired as a z-stack every 30seconds to enable subsequent
248 Weiner filter deconvolution (CellR). A single z-plane is selected for the overlay time series shown
249 with post processing (time stamping and compression) for publication using Videomach
250 (gromeda.com).
251
252 **Results**
253 **(I) Engineering the RedMIT-GFP-LC3 mouse**
254 In order to visualize mitochondrial fate, we first generated a mouse expressing mRFP fused to the
255 COX VIII mitochondrial targeting sequence (figure 1), engineered by random insertion into
256 embryonic stem cells. Mice that were homozygous for the insert, located in the *pkn1* gene (figure S1)
257 appear to be normal with no noticeable effects observed on lifespan or litter size.
258 We confirmed the mitochondrial localization of mRFP in MEFs derived from these mice (figure 1)
259 and observed an O_2 consumption similar to that of wild type MEFs, suggesting that genetic
260 modification had not significantly affected mitochondrial function (figure 2A).

261 To visualize mitochondria specific autophagy, i.e. mitophagy, we crossed this mouse model with the
262 previously described mouse expressing LC3, the hallmark of autophagosomes, tagged with GFP
263 protein (Mizushima et al., 2004). This double fluorescent labelling had no noticeable effect on mice,
264 either reproduction (Table S1), lifespan or litter size.
265 Then we generated MEFs and imaged them using the high throughput imaging system employed
266 previously (Diot et al., 2015) to explore mitochondrial dynamics, autophagy and mitophagy in this
267 mouse model (figures 2B and 2C). Like oxygen consumption (figure 2A), cell growth (not shown)
268 was not affected by the expression of the two fluorescent markers. We routinely CCCP to uncouple
269 mitochondria as a positive control for oxygen consumption. Given the non-significant trend to lower
270 uncoupled respiration in the RedMit/LC3-GFP MEFs, we have not excluded a subtle defect.
271 MEFs were treated with CCCP (carbonyl cyanide m-chlorophenyl hydrazone) to induce mitophagy
272 or with chloroquine to block the final step of the autophagy pathway and analyzed using our IN Cell
273 system (figure 2B). We showed that an induction of mitophagy, or a block in the late stages of
274 mitophagy both result in an increase in the mitophagy signal detected (colocalisation of
275 mitochondrial fragments with autophagosomes, figure 2, p<0.05), consistent with previous results
276 (Diot et al., 2015).
277 As with other cell types, MEFs responded to growth in glucose-free galactose media and starvation
278 media by an induction of mitophagy and mitochondrial fragmentation (Malik et al., 2017). Because
279 the basal level of mitophagy in glucose-free, galactose-based media, is frequently higher than in
280 media containing glucose (but NS in figure 2B) we run our assay in both regular and galactose-based
281 media. Using chloroquine to inhibit lysosomal acidification (25 µM for 16 hours) thus blocking the
282 late steps of the auto/mitophagy pathway, we induced a similar accumulation of mitochondria
283 colocalising with autophagosomes in galactose and glucose- containing media (figure 2C. Data were
284 normalized by log transformation prior to ANOVA. Chloroquine significantly increased
285 colocalisation of mitochondrial fragments with autophagosomes expressed as a proportion of
286 mitochondrial area, p<0.01, effect of galactose NS).
287
288 Finally, we used confocal microscopy to confirm and illustrate our observations with better quality
289 pictures than the ones produced with the high throughput imaging system. Figure 3 illustrates
290 autophagosomes engulfing mitochondria in cells grown in glucose-free galactose media. These cells
291 can be monitored in real time using time lapse imaging, as we did not observe any significant
292 bleaching of the fluorescent signals when the cells were imaged every 30 seconds for 8 hours,
293 enabling tracking of mitophagy in living cells (movie figure S2).
294
295 Together these results confirm that MEFs from the RedMIT-GFP-LC3 mouse are a useful model for
296 the *in vitro* assessment of mitochondrial dynamics.
297
298 **II) The RedMIT-GFP-LC3-OPA1^{Q285STOP} mouse**
299 We previously showed that mitophagy is increased in fibroblasts from patients with bi-allelic OPA1
300 mutations (compound heterozygotes (Liao et al., 2017)). In order to understand the mechanisms
301 underlying this mitophagy dysregulation we crossed our RedMIT-GFP-LC3 mouse with a model of
302 the DOA disease, the OPA1^{Q285STOP} mouse. It is already known that autophagosomes are increased in
303 RGCs in the OPA1^{Q285STOP} mouse (White et al., 2009) and electron microscopy suggests increased
304 mitophagy (Sarzi et al., 2012). But to our knowledge, it is not yet clear whether mitophagic flux is
305 increased. We previously observed increased mitophagy in fibroblasts from ADOA patients in
306 whom we had demonstrated OPA1 deficiency, and therefore wished to explore whether mitophagy
307 was increased in the OPA1^{Q285STOP} mouse model, potentially explaining the increased
308 autophagosomes in RGCs. We generated RedMIT-GFP-LC3-OPA1^{Q285STOP} MEFs, to investigate the
309 effects of OPA1 knock down on autophagy and mitophagy (figure 4). We confirmed that the

310   abundance of OPA1 in the resulting MEFs (figure S3) was lower than in OPA1 wild type MEFs, as
311   expected (Davies et al., 2007). Increased counts of colocalised mitochondria with autophagosomes in
312   the OPA1+/- MEFs (figure 4A) suggested increased mitophagy. Because this increased
313   colocalisation could be due to either activated mitophagy or slowed turnover we assessed mitophagic
314   flux by adding lysosomal inhibitors. We thus blocked the late steps of the autophagy pathway using
315   E64d and pepstatin A over a time-course of 24 hours (figure 4B).
316

317   The accumulation of autophagosomes (expressed as the summed area of LC3-ll positive punctae per
318   cell) is significantly greater in the OPA1 mutant compared to the OPA1 wt (n=3) as shown in figure
319   4A-B. This increase was significant ($p<0.01$, Data were normalized by log transformation prior to
320   ANOVA). As the area of autophagy detected is similar in both the OPA1 wild type and mutant at
321   baseline, but is greater in the OPA1 mutant following inhibitors, this indicates that in steady state
322   conditions, the flux of autophagy is increased in the OPA1 mutant cells compared to the wild type.
323   Similarly, the lysosomal inhibitors significantly increased colocalisation of mitochondrial fragments
324   with autophagosomes expressed as a proportion of mitochondrial area (figure 4C) in the OPA1
325   mutant cells ($p<0.01$, effect of galactose NS). This result is consistent with our previous results in
326   fibroblasts from patients with bi-allelic OPA1 mutations of OPA1 (Liao et al., 2017).
327

328   Together these results show that the OPA1^{Q285STOP} mutation dysregulates both autophagy and
329   mitophagy. Hence this mouse model is useful for studying the underlying mechanisms of the
330   dysregulated mitophagy induced by OPA1 dysfunction in isolated cells.
331

332   **III) Investigation of fixed mouse splenocytes**
333   In order to assess these effects in whole organisms we investigated mouse splenocytes, since large
334   numbers of cells can readily be harvested. This time we used Imagestream, another high content
335   imaging system, in which FACS is coupled to a fluorescence microscope, to investigate
336   colocalisation of mitochondria and autophagosomes. We had previously validated this method for
337   detecting mitophagy in human fibroblasts (Liao et al., 2017). Briefly, the sorted and individualized
338   splenocytes in the flow cytometer are imaged with an integrated fluorescence microscope. The
339   pictures are then analyzed using masks and the colocalisation between mitochondria and
340   autophagosomes assessed. Again, we demonstrated a significantly higher level of colocalisation in
341   OPA1 mutants compared to OPA1 wild type ($p<0.01$, figure 5). This result confirms the induction of
342   mitophagy by the OPA1^{Q285STOP} mutation in the mouse. We therefore investigated the organ mainly
343   affected by dysregulated mitophagy, i.e the retina.
344

345   **IV) Mouse retina investigation**
346   As DOA affects the retinal ganglion cells we investigated autophagy and mitophagy in the retina. For
347   this, four samples from the RedMIT-GFP-LC3-OPA1^{Q285STOP} mice and the RedMIT-GFP-LC3
348   control mice were harvested after fixation by perfusion. Cryostat eye sections were cut at 10 µm and
349   examined using a Zeiss LSM 700 inverted confocal microscope with a plan-Apo 63x NA 1.4 oil-
350   immersion objective. The GFP, which was expected to be targeted to autophagosomes, was
351   homogenously and non-specifically expressed throughout the retinal tissue, as was the mRFP
352   fluorescent mitochondrial signal (figure 6). Furthermore, the expression levels of fluorescent proteins
353   were weak. The results from each slide were very similar; it was not possible to conclude that
354   colocalisation between the GFP and mRFP occurred, as the image signal-to-background ratios
355   precluded the detection of colocalisation with a Pearson correlation coefficient values being either
356   very weakly negative, or very weakly positive. Indeed, the maximum Pearson product moment
357   correlation coefficient values recorded across all four slides were +0.22 and -0.16. We did not detect

358 consistent differences in other tissues examined (figure S4). In summary, the high background and
359 the weak red transgene expression precluded any significant colocalisation analysis.
360
361
362 **Discussion**
363 *Mouse model demonstrates increased mitophagy in primary cell cultures*
364 We have developed a mouse with genetically encoded fluorescent proteins mRFP and GFP directed
365 to mitochondria and autophagosomes respectively (figure 1). We have shown that colocalisation of
366 these tags can be used as a readout for mitophagy in live cells (figure 2), using two different high
367 throughput imaging systems (figures 4 and 5). In live cells from the well characterized mouse model
368 of ADOA (OPA1 ^{Q285STOP}) (Davies et al., 2007) which develops an adult-onset dendropathy and
369 impaired vision, we have shown that baseline mitophagy is increased in splenocytes (figure 5) and
370 mitophagic flux is increased in MEFs (figure 4). Colocalisation of mitochondria with
371 autophagosomes was investigated in retina using confocal microscopy (10 μm cryostat sections).
372
373 These data validate both our model and our high throughput imaging method for quantifying
374 mitophagy. They are consistent with our suggestion that OPA1 knock down causes an excessive
375 mitochondrial fragmentation, and that this activates mitophagy (Liao et al., 2017).
376
377 *This model visualises an earlier stage in mitophagy than do other mouse models*
378 There are considerable technical difficulties with visualizing mitophagy, because it is transient and
379 occurs at low frequency. We set up the high throughput imaging system for quantifying mitophagy
380 in cells (Diot et al., 2015) that we have used in this study. In order to study the mechanisms
381 underlying pathogenesis further, with a view to testing therapeutic strategies *in vivo*, we decided to
382 develop a mouse model allowing us *in vivo* imaging of mitophagy. All three models employed to
383 date use genetic manipulation to express fluorophores (McWilliams et al., 2016; Sun et al., 2015).
384 While two of these can be used both in live and fixed cells, the mt-Keima is not compatible with
385 fixation. The RedMIT-GFP-LC3 mouse model visualizes mitochondrial fragments engulfed by
386 autophagosomes, at an earlier time point in mitophagy than the other mouse models that use mt-
387 Keima and mCherry, which demonstrate fusion with lysosomes. Our model thus complements the
388 previously published models (McWilliams et al., 2016; Sun et al., 2015), which are steady state and
389 endpoint assays, respectively. Both the mt-Keima and the mCherry constructs are functionally inert,
390 but our GFP tag is linked to expression of LC3, an important part of the mitophagy process.
391 Furthermore, our study is limited by our use of the EF1α promoter which drives expression of mRFP.
392 While this promoter is suitable for studies of developing embryos, being ubiquitous in most cell types
393 (Chambers et al., 1998), it is less suitable for studies of post-mitotic tissues such as muscle. Hence
394 the mitochondria of post-mitotic tissues were poorly visualized using mRFP alone, after post-natal
395 day 40.
396
397 While we are able to demonstrate increased mitophagic flux in primary cultures, it is not easy to
398 demonstrate this in whole animals using any of the existing models (McWilliams et al., 2016; Sun et
399 al., 2015).
400
401 *Microscopic examination of tissue sections added no support to data from primary cultures*
402 Despite excellent technical input, we were unable to visualize the colocalisation of mitochondria and
403 autophagosomes, that was apparent in MEFs and splenocytes, in cryostat sections of retina or other
404 tissues. We consider three possible explanations for this. Firstly, our model is not sufficiently
405 sensitive. On fusion with lysosomes, green fluorescent protein is bleached by a drop in pH.
406 Colocalization of the GFP and mRFP signals is therefore short lived. This appears less problematic in

407 cultured cells, where levels of mitophagic flux can be increased by activators, than it is in fixed tissue
408 sections, where colocalization events are less frequent and the signal-to-background ratio sub-
409 optimal. Secondly there are many different subtypes of mitophagy (Lemasters, 2014) and we do not
410 yet know whether the read-out of our high throughput imaging method, that increases with OPA1
411 knockdown (Liao et al., 2017), is BNIP3 dependent. Thirdly, it is possible that mitophagy is not
412 actually increased in retinal ganglion cells in OPA1 knock down. Indeed, Belenguer showed that
413 BNIP3 dependent mitophagy is actually decreased in a neuronal model of OPA1 knock-down
414 (Moulis et al., 2017). Given that we previously showed that mitophagy declines with maturity in
415 fibroblasts (Diot et al., 2015), we suggest that their neuronal cultures may not reflect *in vivo* mature
416 retinal ganglion cells.
417
418 *The importance of activated mitophagy in ADOA*
419 Up until now, much of the evidence for increased mitophagy in ADOA has been indirect. Electron
420 microscopy of retinal ganglion cells is consistent with increased autophagy (White et al., 2009).
421 OPA1 knock down in cultured primary cortical neurons impairs maturation, resulting in reduced
422 mtDNA and abundance of cytochrome oxidase (Bertholet et al., 2013), consistent with, but not
423 attributed to, activated mitophagy. Using the same system other authors have suggested that BNIP3-
424 dependent mitophagy may be decreased rather than increased in OPA1 knock down (Moulis et al.,
425 2017), but these authors did not measure mitophagic flux. We postulate that the increase in
426 mitophagy that we have demonstrated may be different from the BNIP3-dependent type studied by
427 Belenguer (Moulis et al., 2017) as we have never detected accumulation of Parkin. The latter appears
428 to require profound depolarization to a level that does not occur *in vivo*. Furthermore, it has become
429 increasingly clear that there are more than one, and potentially several different types of mitophagy.
430 Some of these are dependent on (Eid et al., 2016b), and others are independent of, PINK1/Parkin
431 (Lemasters, 2014). Indeed, recent data show that PINK1/Parkin knockdown do not diminish basal
432 mitophagy, even in dopaminergic cells, in ether mice (McWilliams et al., 2018) or flies (Lee et al.,
433 2018). Hence their role may be confined to specific stresses (Eid et al., 2016b) and/or differentiation
434 (Sarraf and Youle, 2018).
435
436 The severe phenotypes caused by mutations in genes regulating mitochondrial dynamics highlight the
437 importance of mitochondrial fusion and fission in maintaining cellular, particularly neuronal, health
438 (O'Mealey et al., 2017; Schwarz, 2013). Many disorders of mitochondrial dynamics involve
439 neurodegeneration, including central (Dombi et al., 2016; Haack et al., 2016; Ryan et al., 2015) and
440 peripheral nervous system (Liao et al., 2017; Züchner et al., 2006) as well as severe malformation
441 syndromes (Cullup et al., 2013). While mechanisms of cellular aging are clearly important (Diot et
442 al., 2016; Lang et al., 2017), the precise cause of the neurodegeneration is rarely clear.
443 While increased mitophagy may exert effects on local energy supply within the cell, it is increasingly
444 apparent that significant mitochondrial stresses can be signaled to other parts of the cell. For
445 instance, the UPRmt is a stress response pathway acting as a "checkpoint" for mitochondrial fitness
446 that signals the nucleus (Callegari and Dennerlein, 2018). Acute and chronic mitochondrial
447 respiratory chain deficiency differentially regulate lysosomal biogenesis (Raimundo et al., 2016).
448 Signaling of the acute response requires both TFEB and AMPK. Given that OXPHOS deficiency
449 also results in AMPK-dependent mitochondrial fragmentation (Toyama et al., 2016), mitochondrial
450 dynamics could contribute to the lysosomal response. In the case of OPA1 (Sarzi et al., 2018),
451 mitochondrial fragmentation is apparent before loss of dendrites in retinal ganglion cells while
452 mitochondrial membrane potential is maintained (Williams et al., 2010). Hence delivery of
453 mitochondria to the regions of the cell requiring energy may be as important as mitochondrial
454 quality. OPA1 levels affect mitochondrial membrane cristae structure (Alavi et al., 2007) and
455 potentially impact on apoptosis, though this in not apparent in fibroblasts (Liao et al., 2017). Others

456 have suggested that OPA1 might be important for mtDNA maintenance (Elachouri et al., 2011) but it
457 does not appear to be a component of the nucleoid. We documented mtDNA depletion in OPA1
458 knock down and suggest that this is caused by excessive mitochondrial fragmentation increasing
459 mitophagy beyond the level that it is able to maintain mitochondrial quality. This may recapitulate
460 the excessive mitophagy seen in fibroblasts treated with phenanthroline. This treatment depleted
461 mtDNA copy number to 15% of baseline along with a halving in mitochondrial mass without a
462 significant benefit to the quality of mtDNA (Diot et al., 2015). Activated mitophagy may thus
463 become excessive in its demands on mitochondrial biogenesis, by potentially impairing the ability of
464 the retinal ganglion cells to generate sufficient mitochondria for dendritic growth and/or response to
465 stress.
466
467 *Conclusion*
468 In conclusion, we developed the RedMIT-GFP-LC3 mouse model in which colocalization of
469 fluorescent mitochondria and autophagosomes can be used as a readout to detect mitophagy. We
470 used this model to confirm that mitophagy is increased in cell cultures of a mouse model of ADOA.
471 Autophagy is critically important for optic nerve survival (Rodríguez-Muela et al., 2012) and
472 increased mitophagy may generate cellular demands that are important in neurodegeneration. This
473 model will thus be useful for further studies of neurodegeneration caused by impaired mitochondrial
474 dynamics.
475

484 **Conflict of interest**
485 The authors declare no conflict of interest
486

487 **References**

488 Alavi, M.V., Bette, S., Schimpf, S., Schuettauf, F., Schraermeyer, U., Wehrl, H.F., Ruttiger, L.,
489 Beck, S.C., Tonagel, F., Pichler, B.J., et al. (2007). A splice site mutation in the murine Opa1 gene
490 features pathology of autosomal dominant optic atrophy. Brain J. Neurol. *130*, 1029–1042.

491 Barlow, A.L., Macleod, A., Noppen, S., Sanderson, J., and Guérin, C.J. (2010). Colocalization
492 analysis in fluorescence micrographs: verification of a more accurate calculation of pearson's
493 correlation coefficient. Microsc. Microanal. Off. J. Microsc. Soc. Am. Microbeam Anal. Soc.
494 Microsc. Soc. Can. *16*, 710–724.

495 Bertholet, A.M., Millet, A.M.E., Guillermin, O., Daloyau, M., Davezac, N., Miquel, M.-C., and
496 Belenguer, P. (2013). OPA1 loss of function affects in vitro neuronal maturation. Brain J. Neurol.
497 *136*, 1518–1533.

498 Boya, P. (2017). Why autophagy is good for retinal ganglion cells? Eye Lond. Engl. *31*, 185–190.

499 Callegari, S., and Dennerlein, S. (2018). Sensing the Stress: A Role for the UPRmt and UPRam in
500 the Quality Control of Mitochondria. Front. Cell Dev. Biol. *6*.

501 Chambers, D.M., Peters, J., and Abbott, C.M. (1998). The lethal mutation of the mouse wasted (wst)
502 is a deletion that abolishes expression of a tissue-specific isoform of translation elongation factor
503 1alpha, encoded by the Eef1a2 gene. Proc. Natl. Acad. Sci. U. S. A. *95*, 4463–4468.

504 Chen, H., and Chan, D.C. (2006). Critical dependence of neurons on mitochondrial dynamics. Curr.
505 Opin. Cell Biol. *18*, 453–459.

506 Civiletto, G., Varanita, T., Cerutti, R., Gorletta, T., Barbaro, S., Marchet, S., Lamperti, C., Viscomi,
507 C., Scorrano, L., and Zeviani, M. (2015). Opa1 overexpression ameliorates the phenotype of two
508 mitochondrial disease mouse models. Cell Metab. *21*, 845–854.

509 Cullup, T., Kho, A.L., Dionisi-Vici, C., Brandmeier, B., Smith, F., Urry, Z., Simpson, M.A., Yau, S.,
510 Bertini, E., McClelland, V., et al. (2013). Recessive mutations in EPG5 cause Vici syndrome, a
511 multisystem disorder with defective autophagy. Nat. Genet. *45*, 83–87.

512 Davies, V.J., Hollins, A.J., Piechota, M.J., Yip, W., Davies, J.R., White, K.E., Nicols, P.P., Boulton,
513 M.E., and Votruba, M. (2007). Opa1 deficiency in a mouse model of autosomal dominant optic
514 atrophy impairs mitochondrial morphology, optic nerve structure and visual function. Hum. Mol.
515 Genet. *16*, 1307–1318.

516 Demaison, C., Parsley, K., Brouns, G., Scherr, M., Battmer, K., Kinnon, C., Grez, M., and Thrasher,
517 A.J. (2002). High-level transduction and gene expression in hematopoietic repopulating cells using a
518 human immunodeficiency [correction of imunodeficiency] virus type 1-based lentiviral vector
519 containing an internal spleen focus forming virus promoter. Hum. Gene Ther. *13*, 803–813.

520 Diot, A., Hinks-Roberts, A., Lodge, T., Liao, C., Dombi, E., Morten, K., Brady, S., Fratter, C.,
521 Carver, J., Muir, R., et al. (2015). A novel quantitative assay of mitophagy: Combining high content
522 fluorescence microscopy and mitochondrial DNA load to quantify mitophagy and identify novel
523 pharmacological tools against pathogenic heteroplasmic mtDNA. Pharmacol. Res. *100*, 24–35.

524 Diot, A., Morten, K., and Poulton, J. (2016). Mitophagy plays a central role in mitochondrial ageing.
525 Mamm. Genome Off. J. Int. Mamm. Genome Soc. *27*, 381–395.

526 Dombi, E., Diot, A., Morten, K., Carver, J., Lodge, T., Fratter, C., Ng, Y.S., Liao, C., Muir, R.,
527 Blakely, E.L., et al. (2016). The m.13051G>A mitochondrial DNA mutation results in variable
528 neurology and activated mitophagy. Neurology *86*, 1921–1923.

529 Eid, N., Ito, Y., and Otsuki, Y. (2016a). Triggering of Parkin Mitochondrial Translocation in
530 Mitophagy: Implications for Liver Diseases. Front. Pharmacol. *7*.

531 Eid, N., Ito, Y., Horibe, A., and Otsuki, Y. (2016b). Ethanol-induced mitophagy in liver is associated
532 with activation of the PINK1-Parkin pathway triggered by oxidative DNA damage. Histol.
533 Histopathol. *31*, 1143–1159.

534 Elachouri, G., Vidoni, S., Zanna, C., Pattyn, A., Boukhaddaoui, H., Gaget, K., Yu-Wai-Man, P.,
535 Gasparre, G., Sarzi, E., Delettre, C., et al. (2011). OPA1 links human mitochondrial genome
536 maintenance to mtDNA replication and distribution. Genome Res. *21*, 12–20.

537 Haack, T.B., Ignatius, E., Calvo-Garrido, J., Iuso, A., Isohanni, P., Maffezzini, C., Lönnqvist, T.,
538 Suomalainen, A., Gorza, M., Kremer, L.S., et al. (2016). Absence of the Autophagy Adaptor

539 SQSTM1/p62 Causes Childhood-Onset Neurodegeneration with Ataxia, Dystonia, and Gaze Palsy.
540 Am. J. Hum. Genet. *99*, 735–743.

541 Lang, A., Anand, R., Altinoluk-Hambüchen, S., Ezzahoini, H., Stefanski, A., Iram, A., Bergmann, L.,
542 Urbach, J., Böhler, P., Hänsel, J., et al. (2017). SIRT4 interacts with OPA1 and regulates
543 mitochondrial quality control and mitophagy. Aging *9*, 2163–2189.

544 Lee, J.J., Sanchez-Martinez, A., Zarate, A.M., Benincá, C., Mayor, U., Clague, M.J., and Whitworth,
545 A.J. (2018). Basal mitophagy is widespread in Drosophila but minimally affected by loss of Pink1 or
546 parkin. J. Cell Biol. *217*, 1613–1622.

547 Legros, F., Lombès, A., Frachon, P., and Rojo, M. (2002). Mitochondrial fusion in human cells is
548 efficient, requires the inner membrane potential, and is mediated by mitofusins. Mol. Biol. Cell *13*,
549 4343–4354.

550 Lemasters, J.J. (2014). Variants of mitochondrial autophagy: Types 1 and 2 mitophagy and
551 micromitophagy (Type 3). Redox Biol. *2*, 749–754.

552 Li, Z., Okamoto, K.-I., Hayashi, Y., and Sheng, M. (2004). The importance of dendritic mitochondria
553 in the morphogenesis and plasticity of spines and synapses. Cell *119*, 873–887.

554 Liao, C., Ashley, N., Diot, A., Morten, K., Phadwal, K., Williams, A., Fearnley, I., Rosser, L.,
555 Lowndes, J., Fratter, C., et al. (2017). Dysregulated mitophagy and mitochondrial organization in
556 optic atrophy due to OPA1 mutations. Neurology *88*, 131–142.

557 Malik, S., Diot, A., Morten, K., Dombi, E., Vatish, M., Boyd, C.A.R., and Poulton, J. (2017). Acute
558 nutritional stress during pregnancy affects placental efficiency, fetal growth and adult glucose
559 homeostasis. Oncotarget *8*, 109478–109486.

560 McWilliams, T.G., Prescott, A.R., Allen, G.F.G., Tamjar, J., Munson, M.J., Thomson, C., Muqit,
561 M.M.K., and Ganley, I.G. (2016). mito-QC illuminates mitophagy and mitochondrial architecture in
562 vivo. J. Cell Biol. *214*, 333–345.

563 McWilliams, T.G., Prescott, A.R., Montava-Garriga, L., Ball, G., Singh, F., Barini, E., Muqit,
564 M.M.K., Brooks, S.P., and Ganley, I.G. (2018). Basal Mitophagy Occurs Independently of PINK1 in
565 Mouse Tissues of High Metabolic Demand. Cell Metab. *27*, 439–449.e5.

566 Mizushima, N., Yamamoto, A., Matsui, M., Yoshimori, T., and Ohsumi, Y. (2004). In vivo analysis
567 of autophagy in response to nutrient starvation using transgenic mice expressing a fluorescent
568 autophagosome marker. Mol. Biol. Cell *15*, 1101–1111.

569 Moulis, M.F., Millet, A.M., Daloyau, M., Miquel, M.-C., Ronsin, B., Wissinger, B., Arnauné-
570 Pelloquin, L., and Belenguer, P. (2017). OPA1 haploinsufficiency induces a BNIP3-dependent
571 decrease in mitophagy in neurons: relevance to Dominant Optic Atrophy. J. Neurochem. *140*, 485–
572 494.

573 O'Mealey, G.B., Plafker, K.S., Berry, W.L., Janknecht, R., Chan, J.Y., and Plafker, S.M. (2017). A
574 PGAM5-KEAP1-Nrf2 complex is required for stress-induced mitochondrial retrograde trafficking. J.
575 Cell Sci. *130*, 3467–3480.

576 Raimundo, N., Fernández-Mosquera, L., Yambire, K.F., and Diogo, C.V. (2016). Mechanisms of
577 communication between mitochondria and lysosomes. Int. J. Biochem. Cell Biol. *79*, 345–349.

578 Rodríguez-Muela, N., Germain, F., Mariño, G., Fitze, P.S., and Boya, P. (2012). Autophagy
579 promotes survival of retinal ganglion cells after optic nerve axotomy in mice. Cell Death Differ. *19*,
580 162–169.

581 Ryan, B.J., Hoek, S., Fon, E.A., and Wade-Martins, R. (2015). Mitochondrial dysfunction and
582 mitophagy in Parkinson's: from familial to sporadic disease. Trends Biochem. Sci. *40*, 200–210.

583 Sarraf, S.A., and Youle, R.J. (2018). Parkin mediates mitophagy during beige-to-white fat
584 conversion. Sci Signal *11*, eaat1082.

585 Sarzi, E., Angebault, C., Seveno, M., Gueguen, N., Chaix, B., Bielicki, G., Boddaert, N., Mausset-
586 Bonnefont, A.-L., Cazevieille, C., Rigau, V., et al. (2012). The human OPA1delTTAG mutation
587 induces premature age-related systemic neurodegeneration in mouse. Brain J. Neurol. *135*, 3599–
588 3613.

589 Sarzi, E., Seveno, M., Piro-Mégy, C., Elzière, L., Quilès, M., Péquignot, M., Müller, A., Hamel, C.P.,
590 Lenaers, G., and Delettre, C. (2018). OPA1 gene therapy prevents retinal ganglion cell loss in a
591 Dominant Optic Atrophy mouse model. Sci. Rep. *8*, 2468.

592 Schwarz, T.L. (2013). Mitochondrial trafficking in neurons. Cold Spring Harb. Perspect. Biol. *5*.

593 Sun, N., Yun, J., Liu, J., Malide, D., Liu, C., Rovira, I.I., Holmström, K.M., Fergusson, M.M., Yoo,
594 Y.H., Combs, C.A., et al. (2015). Measuring In Vivo Mitophagy. Mol. Cell *60*, 685–696.

595 Suomalainen, A., and Battersby, B.J. (2018). Mitochondrial diseases: the contribution of organelle
596 stress responses to pathology. Nat. Rev. Mol. Cell Biol. *19*, 77–92.

597 Toyama, E.Q., Herzig, S., Courchet, J., Lewis, T.L., Losón, O.C., Hellberg, K., Young, N.P., Chen,
598 H., Polleux, F., Chan, D.C., et al. (2016). Metabolism. AMP-activated protein kinase mediates
599 mitochondrial fission in response to energy stress. Science *351*, 275–281.

600 Varanita, T., Soriano, M.E., Romanello, V., Zaglia, T., Quintana-Cabrera, R., Semenzato, M.,
601 Menabò, R., Costa, V., Civiletto, G., Pesce, P., et al. (2015). The Opa1-Dependent Mitochondrial
602 Cristae Remodeling Pathway Controls Atrophic, Apoptotic, and Ischemic Tissue Damage. Cell
603 Metab. *21*, 834–844.

604 White, K.E., Davies, V.J., Hogan, V.E., Piechota, M.J., Nichols, P.P., Turnbull, D.M., and Votruba,
605 M. (2009). OPA1 deficiency associated with increased autophagy in retinal ganglion cells in a
606 murine model of dominant optic atrophy. Invest. Ophthalmol. Vis. Sci. *50*, 2567–2571.

607 Williams, P.A., Morgan, J.E., and Votruba, M. (2010). Opa1 deficiency in a mouse model of
608 dominant optic atrophy leads to retinal ganglion cell dendropathy. Brain J. Neurol. *133*, 2942–2951.

609 Williams, P.A., Piechota, M., von Ruhland, C., Taylor, E., Morgan, J.E., and Votruba, M. (2012).
610 Opa1 is essential for retinal ganglion cell synaptic architecture and connectivity. Brain J. Neurol.
611 *135*, 493–505.

612 Yu-Wai-Man, P., Turnbull, D.M., and Chinnery, P.F. (2002). Leber hereditary optic neuropathy. J.
613 Med. Genet. *39*, 162–169.

614 Yu-Wai-Man, P., Votruba, M., Moore, A.T., and Chinnery, P.F. (2014). Treatment strategies for
615 inherited optic neuropathies: past, present and future. Eye Lond. Engl. *28*, 521–537.

616 Züchner, S., De Jonghe, P., Jordanova, A., Claeys, K.G., Guergueltcheva, V., Cherninkova, S.,
617 Hamilton, S.R., Van Stavern, G., Krajewski, K.M., Stajich, J., et al. (2006). Axonal neuropathy with
618 optic atrophy is caused by mutations in mitofusin 2. Ann. Neurol. *59*, 276–281.

619

620 **Figure legends**
621 **Figure 1. The RedMIT-GFP-LC3-OPA1^{Q285STOP} mouse.**
622 The RedMIT mouse has been genetically engineered by random insertion of the illustrated construct.
623 The mRFP fluorescent protein is fused to the mitochondrial targeting sequence of COX VIII and its
624 expression perfectly colocalizes with PDH (panel, scale bar = 20μm). Expression is under the control
625 of the EF1α promoter. Homozygous females were then crossed to GFP-LC3 males (Mizushima et al.,
626 2004) to obtain our RedMIT-GFP-LC3 mouse model. Once both fluorescent markers were
627 homozygous, RedMIT-GFP-LC3 mice were crossed to the OPA1^{Q285STOP} mice (White et al., 2009).
628
629 **Figure 2. Validation of the RedMIT-GFP-LC3 Mouse model for detecting mitophagy.**
630 (see Diot et al., 2015 for detailed validation of high throuput imaging to quantify mitophagy)
631 A) MEFs from WT, RedMIT and RedMIT-GFP-LC3 mice were used to clarify whether expressing
632 mRFP in mitochondria impaired their function. No significant differences in oxygen consumption
633 were observed either in glycolytic (Glucose), oxidative (Galactose) or uncoupled (CCCP) conditions
634 (mean + SD, n=2, t-test p=0.625 – 0.684 – 0.289 for wt vs RedMIT-GFP-LC3 / 0.832 – 0.559 – 0.714 for wt
635 vs RedMIT / 0.532 – 0.409 – 0.369 for RedMIT vs RedMIT-GFP-LC3 (glucose – galactose – CCCP,
636 respectively)).
637 B) Using our IN Cell 1000 high-throughput microscopy assay (Diot et al., 2015) we validated
638 detection of mitophagy in RedMIT-GFP-LC3 MEFs grown for 2 hours in glucose media (control),
639 glucose-free galactose-based media (galactose), starvation media (EBSS), media containing vehicle
640 (DMSO), glucose media supplemented with 10μM CCCP (CCCP) and glucose media supplemented
641 with 25μM chloroquine (CQ). After fixation, an increase colocalization between mitochondria and
642 LC3 was observed when using an inhibitor (chloroquine, CQ) of mitophagy, and when using CCCP
643 compared to DMSO control (mean + SEM, at least 500 cells counted per condition, t-test, both
644 p<0.01)
645 C) Using IN Cell 1000, chloroquine significantly increased colocalisation of mitochondrial fragments
646 with autophagosomes expressed as a proportion of mitochondrial area in both regular (glucose) and
647 glucose-free galactose based media (p<0.01, t-test, effect of medium NS, error bars are SE at least
648 500 cells counted)
649
650 **Figure 3. The early stages of mitophagy can readily be demonstrated in RedMIT-GFP-LC3**
651 **MEFs.**
652 RedMIT-GFP-LC3 MEFs were cultured in glucose-free galactose media (galactose). After fixation,
653 the cells were imaged using a Leica SP5 confocal microscope with a 63X lens and further digital
654 zoom when needed. Autophagosomes forming around a mitochondrion are observed under these
655 "energetic stress" growth conditions. Similar observations in whole cells images have been made in
656 (Liao et al., 2017).

657

Figure 4. The OPA1^{Q285STOP} mutation induces mitophagy in MEFs.

A) Representative images of the IN Cell 1000 high content imaging acquisition system. The cells from both RedMIT-GFP-LC3 and RedMIT-GFP-LC3-OPA1^{Q285STOP} were grown in glucose media (0h) supplemented with E64d/Pepstatin A for 6h before fixation. The images are analyzed using a homemade protocol developed using the IN Cell developer toolbox (Diot et al, 2015) resulting in a "mask" picture (cyan: autophagosomes; red: "short" mitochondria; yellow: "long" mitochondria; purple: "colocalisation between autophagosome and mitochondria signals). The white arrows in the insets indicate the colocalisation events between mitochondrial and autophagosome signal.

B) Lysosomal inhibitors E64d/Pepstatin A were added to cells growing in glucose media to block the processing of autophagolysosomes. As shown on the graph a greater accumulation of autophagosomes is observed in MEFs from the RedMITGFP-LC3-OPA1^{Q285TOP} mouse compared to the RedMIT-GFP-LC3-OPA1$^{+/+}$ mouse, indicating a greater flux of autophagy when the OPA1 mutation is present. (at least 500 cells counted, regression p<0.05)

C) In similar conditions, a greater flux of mitophagy (mitochondrial fragments colocalizing with autophagosomes) is observed with the OPA1 mutation: the rate of accumulation of mitophagosomes is 0.73 +/-0.21 (SEM) for wild type and 1.96 +/-0.22 for OPA1. (at least 500 cells counted, regression p<0.02)

675

Figure 5. Baseline mitophagy is increased by the OPA1^{Q285STOP} mutation in mouse splenocytes.

Fixed splenocytes (1000 to 5000 per mouse) from three RedMITGFP-LC3-OPA1^{Q285TOP} mice (designated 1, 2 and 3) and three RedMIT-GFP-LC3 mice (designated 4, 5 and 6) mice were prepared and analysed using the Imagestream (Amnis) system, error bars are SE of technical replicates. In line with the results observed in MEFs, colocalization between mitochondria and LC3 is increased in the OPA1 mutant mice. (t-test p<0.01)

682

Figure 6: Confocal images of transgenic OPA1wt *and* OPA1 Q285STOP mouse retina sections expressing LC3-GFP and RedMIT

Representative images of the retina from the RedMIT-GFP-LC3-OPA1$^{+/+}$ (left) and the RedMIT-GFP-LC3-OPA1^{Q285STOP} (right) mice sections show autophagosomes with GFP-tagged LC3 and RedMIT tagged mitochondria. Sections were cut at 10 µm and visualized using a Zeiss LSM 700 inverted confocal microscope with a plan-Apo 63x NA 1.4 oil-immersion objective. Red boxes indicate the area magnified in each inset. RedMIT were observed from the ONL towards the IPL in both OPA1^{wt} *and* OPA1 ^{Q285STOP}. No difference in GFP-LC3 or mitochondrial mRFP is seen between OPA wild type and mutant (zoomed insets, bottom panels). In particular, no colocalization was observed between GFP-LC3 and RedMIT in both OPA1^{wt} *and* OPA1^{Q285STOP} (Pearson correlation coefficient of +0.22 and -0.16; n=4). Scale bars: 20 µm

OS: outer segments; IS: inner segments; ONL: outer nucleus layer; OPL: outer plexiform layer; INL: inner nucleus layer; IPL: inner plexiform layer; GCL: ganglion cell layer

696

Supplementary information

Figure S1. Mapping of the mRFP transgene

The insertion of the mRFP transgene was investigated by paired-end sequencing. The insert is located in the 3rd exon of the *pkn1* gene, which has been confirmed by PCR using a common forward primer (green) and two different reverse primers; one (red) 1500bp from the forward primer in the wild type genome (blue) and one in the mRFP insert, approximately 800bp from the forward

16

703 primer. The 1500bp PCR only works in the wild type genome and the 800bp only when the insert is
704 present.
705
706 **Figure S2. Movie of the RedMIT-GFP-LC3 MEFs.**
707 Live RedMIT-GFP-LC3 MEFs have been imaged using a custom Olympus IX81 inverted
708 microscope equipped with temperature control (Solent scientific) every 30 seconds for 8 hours. This
709 can be used to quantify the early stages of mitophagy in real time.
710
711 **Figure S3. Analysis of OPA1 expression in the MEFs used**
712 Protein extracts were prepared from wt, RedMIT-GFP-LC3 and RedMIT-GFP-LC3-OPA1^{Q285STOP}
713 MEFs and analyzed on a 8% acrylamide gel. The OPA1 signal was detected using a rabbit anti-
714 OPA1 antibody (abcam ab42364) and revealed using a polyclonal goat anti-rabbit secondary
715 antibody (Dako P0448) coupled to an ECL detection kit (WESTAR® Supernova HRP Detection
716 Substrate, Geneflow K1-0068) according to the manufacturer's instructions and imaged with G:BOX
717 (Syngene).
718
719 **Figure S4. Images from sections of brain and spleen from control, RedMIT/GFP-LC3 and**
720 **OPA1^{Q285STOP}/RedMIT/GFP-LC3.** Brain (bottom) and spleen (top) from non-fluorescent (control),
721 RedMIT/GFP-LC3 and OPA1^{Q285STOP}/RedMIT/GFP-LC3 mice were sectioned (10µm) and imaged
722 on a Zeiss LSM 700 inverted confocal microscope with a plan-Apo 63x NA 1.4 oil-immersion
723 objective. The fluorescent signals, GFP-LC3 and mitochondrial mRFP, are visible but no clear
724 colocalization between them could be visualized in the views shown. High throughput imaging
725 identified infrequent colocalisation that was more marked in OPA1^{Q285STOP}/RedMIT/GFP-LC3 mice
726 than RedMIT/GFP-LC3 mice (figure 5). Scale bars = 10µm
727

Strain	Reproductive index	Pre-wean mortality
RedMIT/GFP-LC3	0.52	31%
RedMIT/GFP-LC3/OPA1	0.59	25%
OPA1+/-	0.56	25%

728
729 Table S1. mRFP and GFP transgenes do not affect mice reproductive success
730
731 **Authors contribution**
732 AD, TA, JS, CL, JC, RN, RG, YG, CW, SS, MD, ED, LM performed the experiments. JP, KM, SW
733 and AD designed the experiments. JP, JS, RC, TL, FI, KM and AD analyzed the results. JP, AD, JS,
734 KM and MD wrote this manuscript.

Figure 1.TIFF
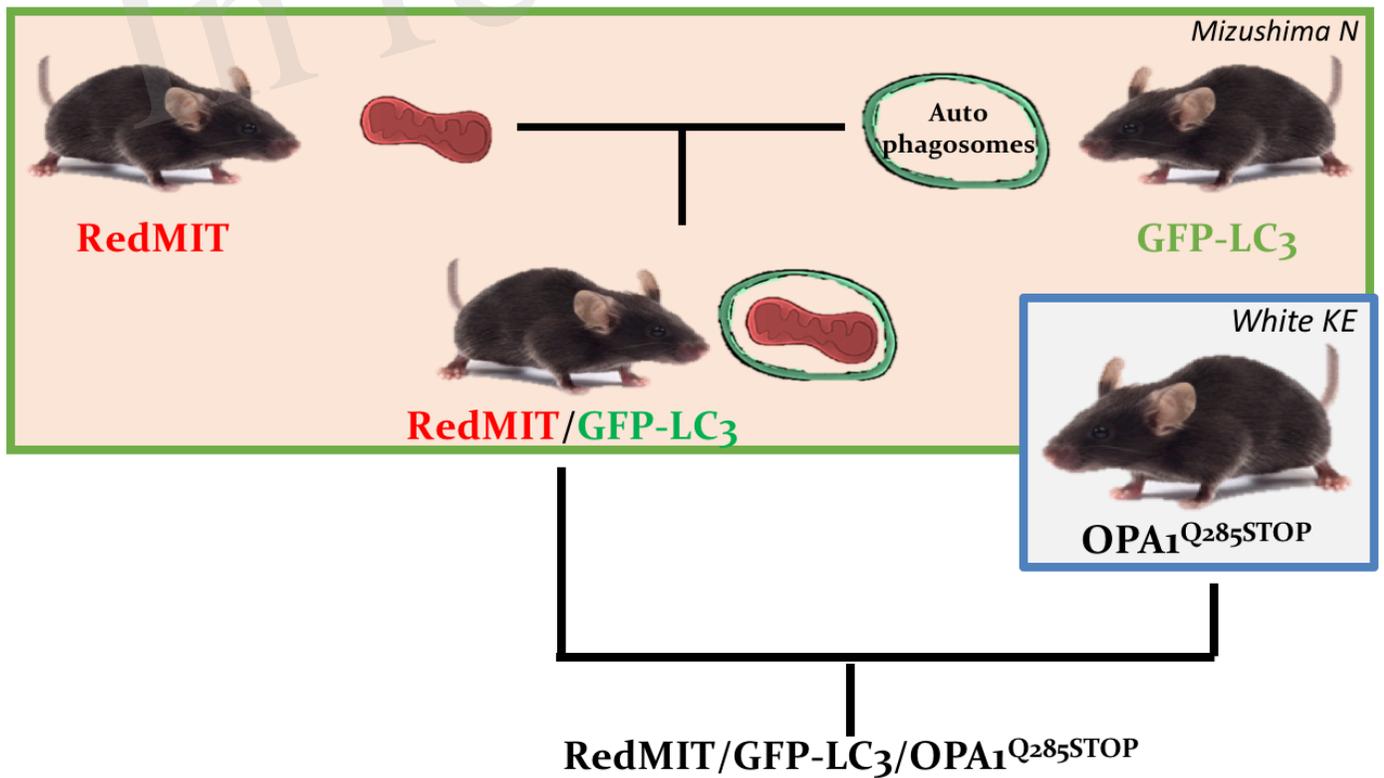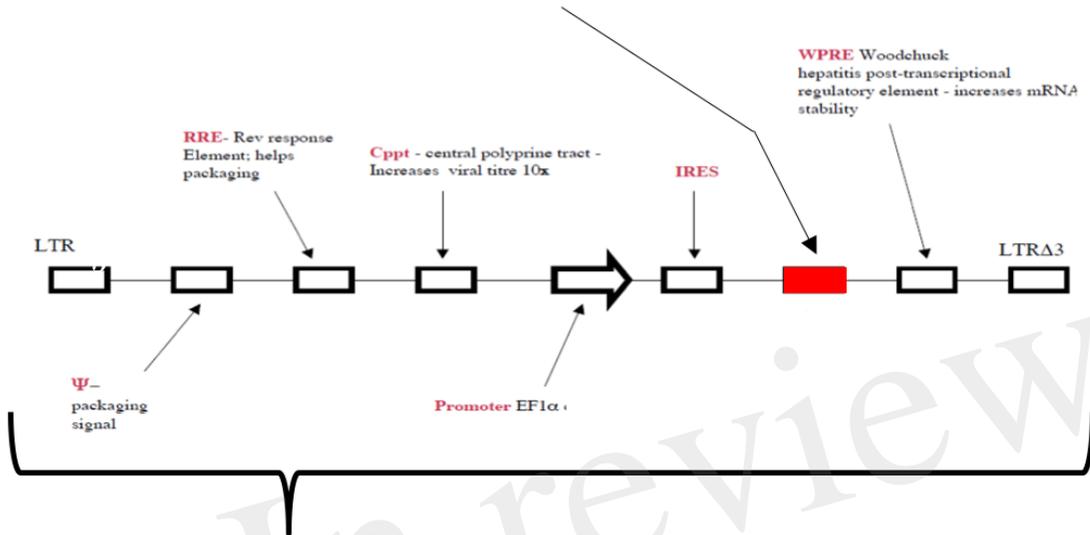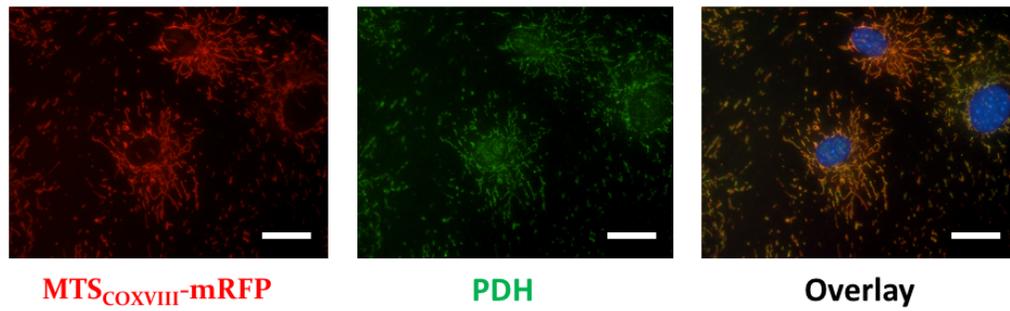
Figure 1. The RedMIT-GFP-LC3-OPA1^{Q285STOP} mouse

Figure 2.TIFF
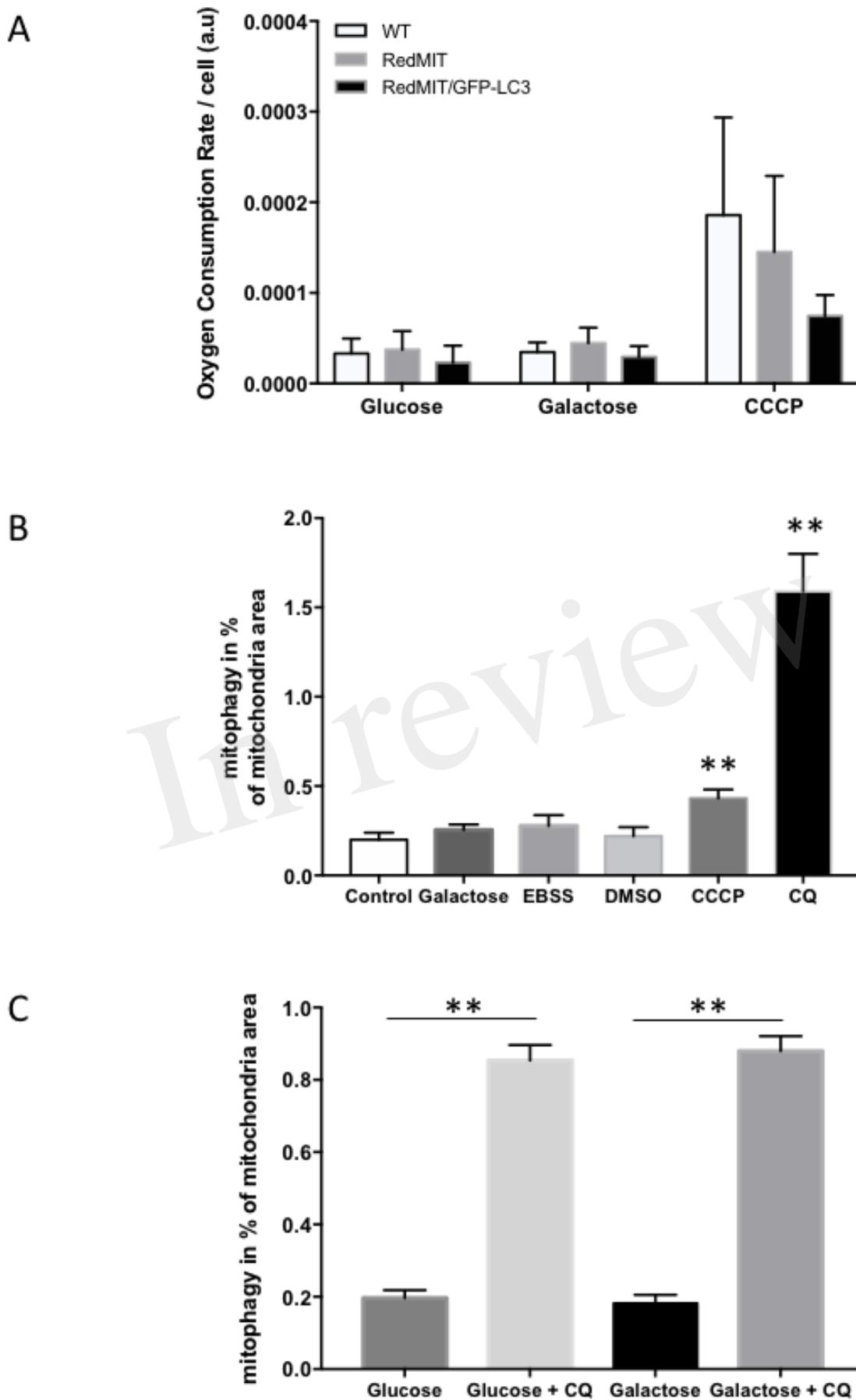
Figure 2. Mouse model to monitor mitophagy validation

Figure 3.TIFF

Mitochondria / LC3
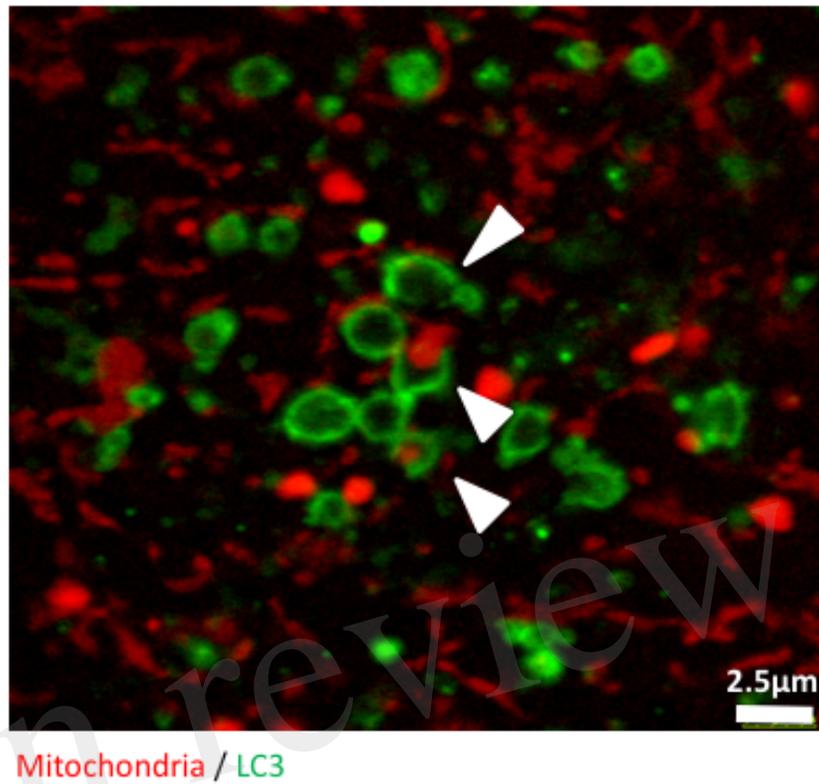
Figure 3. RedMIT-GFP-LC3 MEFs allows for mitophagy early and late steps detection
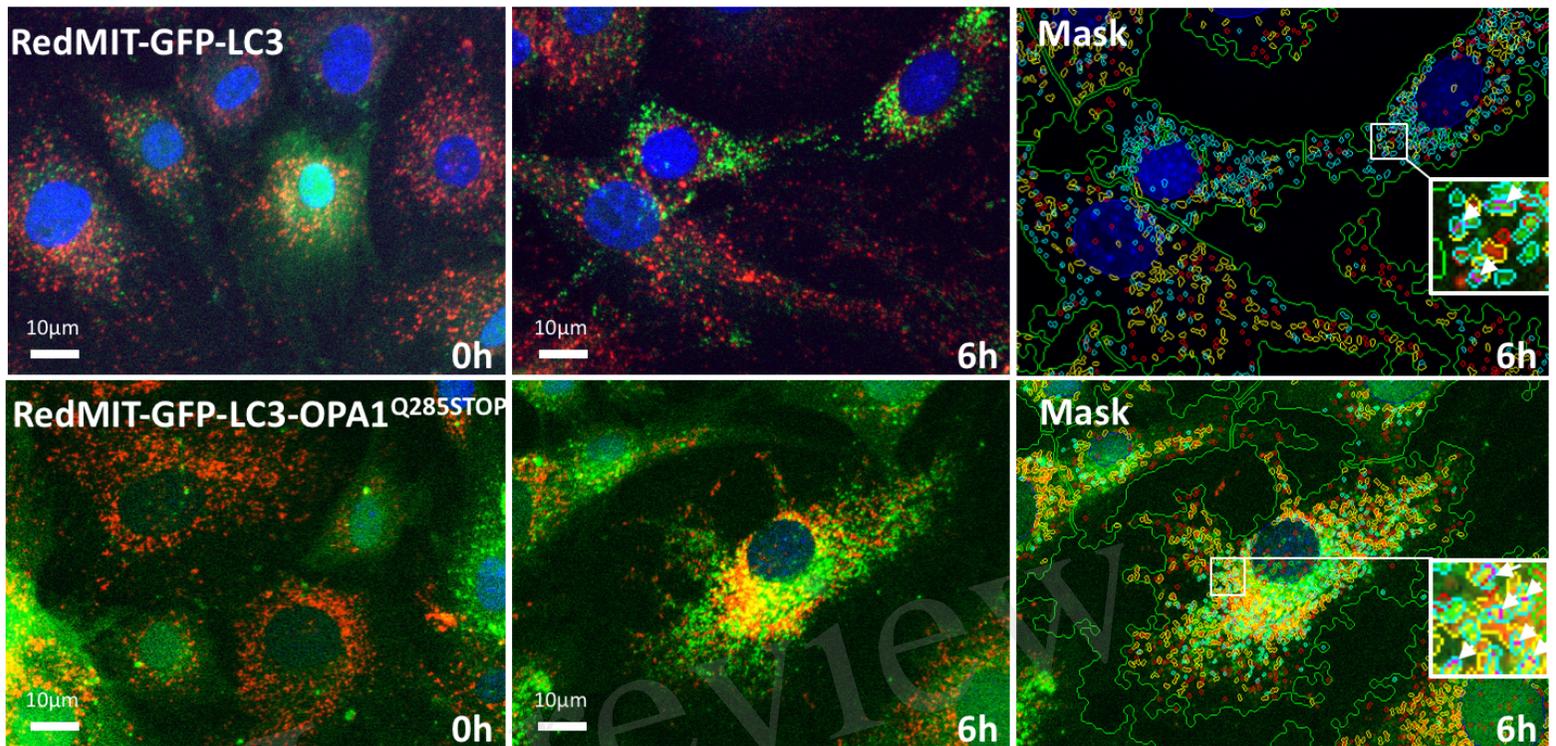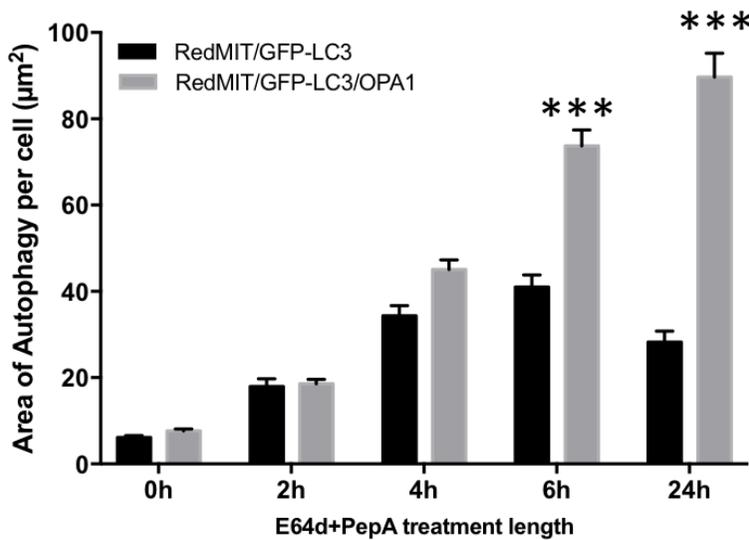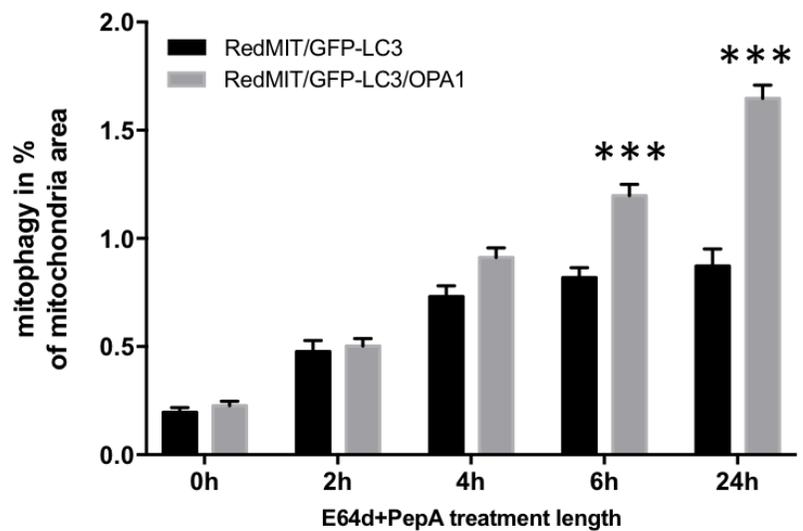
Figure 4.TIFF

Figure 4. The OPA1^{Q285STOP} mutation induces mitophagy in MEFs

Figure 5.TIFF
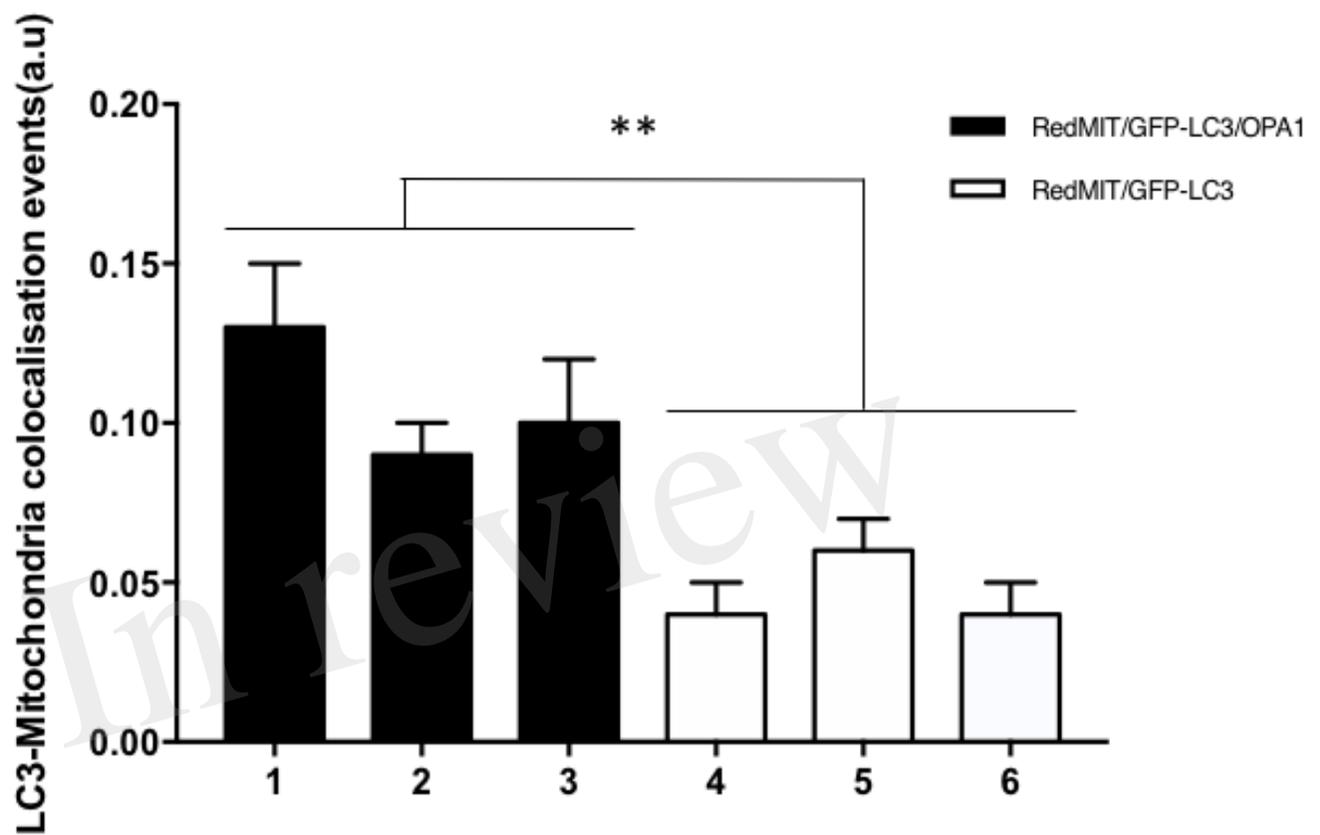
Figure 5. Baseline mitophagy is increased by OPA1^{Q285STOP} mutation in mouse splenocytes

Figure 6.TIF

OPA1^wt

OPA1^Q285STOP

OS
IS
ONL
OPL
INL
IPL
GCL

20 μm

20 μm

20 μm

20 μm